NUCLEAR SCIENCE AND ENGINEERING · VOLUME 193 · 269–282 · MARCH 2019

DOI: https://doi.org/10.1080/00295639.2018.1520526

Neutron Transmission and Capture Measurements of ^{133}Cs from 0.01 to 600 eV

R. C. Block,[a]* J. A. Burke,[a] D. P. Barry,[a] N. J. Drindak,[a†] G. Leinweber,[a] K. E. Remley,[a] R. V. Ballad,[a†] M. J. Rapp,[a] and Y. Danon[b]

[a]*Naval Nuclear Laboratory, P.O. Box 1072, Schenectady, New York 12301-1072*
[b]*Rensselaer Polytechnic Institute, Gaerttner LINAC Center, 110 8th Street, Troy, New York 12180*

Received June 4, 2018
Accepted for Publication September 1, 2018

Abstract — *Neutron capture and transmission measurements were carried out from 0.01 to 600 eV on both solid and liquid samples containing elemental cesium (^{133}Cs). Only s-wave resonances were observed in these measurements. These data were analyzed for resonance parameters utilizing the SAMMY Bayesian analysis code to simultaneously fit both the capture and transmission data. Parameters were obtained for 31 cesium resonances up to 600 eV. The thermal capture cross section and capture resonance integral were determined. The thermal capture cross section is 10% larger than the ENDF, JENDL, and JEFF evaluated values but lies within the uncertainty of the most recent measurement by Yoon and Lee [New Phys.: Sae Mulli (Korean Phys. Soc.)., Vol. 61, p. 7 (2011)]. The capture resonance integral has a statistical 1σ error of 2% and lies 1.4σ above the JENDL value, 5.5σ above the ENDF value, and 3.9σ above the JEFF value. The s-wave strength function was determined.*

Keywords — *Cesium, resonance parameters, thermal capture cross section, capture resonance integral.*

Note — *Some figures may be in color only in the electronic version.*

I. INTRODUCTION

Elemental cesium consists of a single isotope: ^{133}Cs. Cesium is abundantly produced in nuclear reactors where 6.7% of the fissions from ^{235}U ultimately produce ^{133}Cs (Ref. 1). Since neutrons inside a reactor interact with this large amount of material, it is important to have accurate cesium neutron cross sections. Total cross-section measurements[2-5] and capture measurements[6–8] over the resonance energy region have been reported for cesium as well as numerous thermal total cross-section[7,9] and capture measurements.[10–21]

Since almost all of the previous results measured either total or capture cross section separately, it was decided to utilize the transmission and capture experimental facilities at the Rensselaer Polytechnic Institute Gaerttner Linear Accelerator (LINAC) Center to provide a combined total-plus-capture measurement and analysis from thermal energies to 600 eV. Time-of-flight (TOF) transmission measurements were carried out with transmission detectors at the 15-m flight station (0.01 to 30 eV) and 25-m flight station (3 to 600 eV). Capture measurements utilized the 16-section sodium iodide (NaI) multiplicity detector at the 25-m flight station with separate thermal (0.01 to 30 eV) and epithermal (3 to 600 eV) measurements. The data were reduced to neutron transmission and capture yield, and the Bayes analysis code SAMMY (Ref. 22) was used to obtain a set of resonance parameters that best fit all the data.

II. EXPERIMENTAL CONDITIONS

II.A. Overview of Measurements

Transmission and capture measurements were carried out using the TOF method with both liquid [cesium carbonate (Cs_2CO_3) dissolved in D_2O] and solid [cesium fluoride (CsF) crystals] samples of cesium. The experimental details used

*E-mail: blockr@rpi.edu
†Retired

for data acquisition are listed in Table I. The experimental method and details are essentially the same as those reported in detail by Leinweber et al.[23] and will be only briefly described here. The Gaerttner LINAC Center linear accelerator was used to produce energetic electrons, and these electrons, in turn, impinged on water-cooled Ta plates to produce bremsstrahlung photons and then neutrons via the photoneutron reaction. The thermal transmission and capture measurements used the enhanced thermal neutron target[24,25] whereas the epithermal transmission and capture measurements used the bare bounce target.[26] The thermal transmission measurements utilized a 0.3-cm-thick ^{6}Li glass scintillator detector mounted directly on a photomultiplier at the 15-m flight station. The epithermal transmission measurements utilized a 1.27-cm-thick ^{6}Li glass detector at the 25-m flight station with the glass viewed by two photomultipliers located outside of the neutron beam.[27] The thermal and epithermal capture measurements utilized the 16-section NaI multiplicity detector[28] located at the 25-m flight station.

The neutron intensity from the accelerator was monitored with moderated fission chambers located at an ~9-m flight path, a ^{6}Li glass ring detector placed in the epithermal transmission flight tube, and when applicable a ^{6}Li glass detector located at the 15-m flight path. These monitor detectors were used to minimize the effects of beam intensity fluctuations as well as correct for different collection times for the various sample and open positions.

II.B. Sample Information

Two types of samples were used for these measurements: a set of CsF crystals and a set of liquid samples consisting of Cs_2CO_3 dissolved in heavy water (D_2O). The CsF crystals provided thick samples while the liquid samples provided thin samples of uniform thickness. The CsF crystals were grown at Iowa State University and encapsulated in 0.508-mm-thick aluminum cans with 0.0762-mm-thick Mylar films between the crystals and aluminum. The liquid samples were prepared at the Naval Nuclear Laboratory by dissolving Cs_2CO_3 powder in D_2O and sealing the solution into cylindrical quartz cells with 3.81-cm inside diameter and 0.1588-cm-thick windows.

II.B.1. CsF Samples

Three thicknesses of CsF were used for these measurements with nominal thicknesses of 6.86, 20.1, and 25.2 mm. The samples were not rigid solids but were rather somewhat jellylike in consistency. However, they did have two well-defined parallel faces. The sample thicknesses were determined by measuring the outer thickness of the CsF-Mylar-aluminum assembly and subtracting the 1.01-mm aluminum and 0.152-mm Mylar thicknesses. The CsF thickness uncertainty is estimated as ±0.25 mm. Table II lists the atomic number densities of the Cs and F in the crystals and the C, O, and H in the two 0.0762-mm-thick films of Mylar.

II.B.2. Liquid Samples

Cesium carbonate powder was dissolved into heavy water to produce a stock solution, and portions of this stock solution were further diluted with heavy water to produce four cesium liquid samples. Chemical analysis of the powder indicated that it was a mixture of 93.1% Cs_2CO_3 and 6.9% cesium bicarbonate ($CsHCO_3$). This powder also contained 1% water (by weight).

In addition to the Cs samples, two heavy water–filled quartz cylinders were utilized to provide open samples with the same physical thickness as the corresponding Cs samples. The fact that there is more D_2O in the open samples than the Cs samples is taken into account in analyzing these transmission data for resonance parameters. Table III lists the nominal thickness of the liquids in each cell and the atomic number densities of the Cs, C, O, H, and D in these samples (including the 1% water).

These quartz cells had a wall thickness of 1.59 mm. For these measurements the neutron beam impinged perpendicularly on the face of the cylindrically shaped sample.

III. DATA REDUCTION

Transmission and capture measurements were made over two neutron energy regions: thermal and epithermal. The thermal measurements were optimized to take data to be analyzed in the 0.01- to 30-eV energy range, whereas the epithermal measurements emphasized the 3- to 600-eV range. The thermal transmission measurement used all three CsF samples, while only the 6.86-mm sample was used for the capture measurement. The epithermal transmission measurements used all the CsF and liquid samples, while the capture measurements used all the liquid samples but only the 6.86-mm CsF sample.

The method for the reduction of the transmission and capture data was essentially the same as carried out by Leinweber et al.[23] Capture data were reduced to capture yield and transmission data to transmission.

TABLE I

Experimental Details Showing Accelerator and Data Acquisition Parameters

Measurement (Cs Sample)	Overlap Filter	Neutron Target	Electron Pulse Width (μs)	Average Electron Current (μA)	Electron Energy (MeV)	Neutron Energy Region (eV)	Channel Width (μs)	Repetition Rate (pps)	Flight Path (m)
Thermal transmission (crystal)	None	Enhanced thermal	1.0	6.0	54	$E < 0.50$ $0.50 < E < 3.0$ $3.0 < E < 19$ $19 \leq E$	16 0.50 0.25 0.125	25	14.974 ± 0.006
Epithermal transmission (liquid)	B_4C (7.9 mm)	Bare bounce	0.100	26	54	$E < 4.0$ $4.0 < E < 45$ $45 < E < 262$ $262 \leq E$	8 0.50 0.0625 0.03125	225	25.596 ± 0.006
Epithermal transmission (crystal)	B_4C (7.9 mm)	Bare bounce	0.050	19	62	$E < 16$ $16 < E < 84$ $84 < E < 372$ $372 \leq E$	4 0.25 0.0625 0.03125	250	26.868 ± 0.003
Thermal capture (crystal)	None	Enhanced thermal	3.0	16	48	$E < 0.010$ $0.010 < E < 0.049$ $0.049 < E < 2.9$ $2.9 \leq E$	128 32 16 0.5	25	25.444 ± 0.006
Epithermal capture (liquid)	B_4C (7.9 mm)	Bare bounce	0.056	13	67	$E < 15$ $15 < E < 76$ $76 < E < 312$ $312 \leq E$	4 0.25 0.0625 0.03125	250	25.564 ± 0.006
Epithermal capture (crystal)	B_4C (7.9 mm)	Bare bounce	0.056	16	64	$E < 15$ $15 < E < 76$ $76 < E < 333$ $333 \leq E$	4 0.25 0.0625 0.03125	250	25.564 ± 0.006

TABLE II

Atomic Number Densities of the CsF Samples and Mylar Films

Nominal Thickness (mm)	N_{Cs} (atom/b)	N_F (atom/b)	N_C (atom/b)	N_O (atom/b)	N_H (atom/b)
6.86	1.032E–02	1.032E–02	6.860E–04	2.744E–04	5.488E–04
20.1	3.182E–02	3.182E–02	6.860E–04	2.744E–04	5.488E–04
25.2	4.057E–02	4.057E–02	6.860E–04	2.744E–04	5.488E–04

TABLE III

Liquid Thickness and Atomic Number Densities of the Cesium Solution and Heavy Water–Filled Cells

Cell Number	Nominal Liquid Thickness (mm)	N_{Cs} (atom/b)	N_C (atom/b)	N_O (atom/b)	N_H (atom/b)	N_D (atom/b)
Cs-L-3	3.18	7.308E–05	4.865E–05	1.053E–02	3.848E–05	2.076E–02
Cs-L-4	3.18	2.526E–04	1.681E–04	1.093E–02	1.330E–04	2.079E–02
Cs-L-5	3.18	8.711E–04	5.799E–04	1.084E–02	4.586E–04	1.803E–02
Cs-L-7	6.35	2.963E–03	1.972E–03	2.080E–02	1.560E–03	2.919E–02
Cs-L-6	3.18			1.073E–02		2.145E–02
Cs-L-8	6.35			2.107E–02		4.214E–02

III.A. Neutron Energy

The neutron energy at low (nonrelativistic) energies in TOF channel i is given by

$$E_i = \left[\frac{C\,L}{t_i - t_0}\right]^2 , \tag{1}$$

where

E_i = energy (eV)

L = flight path (m)

$(t_i - t_0)$ = TOF (μs)

C = conversion factor = 72.29824.

The recorded time of an event in channel i is t_i while t_0 is the time when the electron pulse strikes the neutron target. By measuring the time when the gamma flash is detected, t_0 is obtained by correcting for the flight time of these gamma rays from the neutron target to the detector.

III.B. Capture Yield

The capture yield Y_i in TOF channel i is calculated by

$$Y_i = \frac{C_i - B_i}{K\,\varphi_{r,i}} , \tag{2}$$

where the numerator refers to the net capture counting rate with the capture sample in the beam and the denominator to the neutron rate incident upon the capture sample. C_i and B_i are the dead-time–corrected and beam-monitor–normalized counting rates with the capture sample in the beam and the background counting rate with either the equal-thickness D_2O sample (for the liquid sample measurements) or empty aluminum can in the beam (for the CsF sample measurements), respectively. The relative neutron flux incident upon the capture sample $\varphi_{r,i}$ was determined from a measurement with a $^{10}B_4C$ sample placed in the neutron beam. These counting data were dead-time corrected and background subtracted. The relative neutron flux is equal to the resulting net counting data divided by the efficiency for detecting the gamma ray from the $^{10}B(n;\alpha,\gamma)$ reaction. The constant K normalizes the relative neutron flux to the actual neutron rate incident upon the capture sample.

The normalization constant K is typically determined by measuring capture in a region where the capture yield Y is known. Cesium has a mostly capture resonance at 5.9 eV, which saturates with all the CsF samples and the thickest liquid sample. This resonance was used to

normalize the CsF sample capture yield in the thermal measurement and the epithermal liquid sample yield in the energy region from 3 to 15 eV. Above 15 eV both the liquid and CsF capture yields were normalized to saturated capture in the 22.5-eV resonance.

Monte Carlo calculations indicated that the presence of Mylar in the CsF capture sample introduced an error in the capture yield that was much smaller than the overall error in the yield. The presence of Mylar also leads to an increase in the thermal capture cross section that is considerably smaller than the overall error in this cross section. Thus, the effect of Mylar upon the capture yield of CsF was ignored in analyzing the CsF capture data.

III.C. Transmission

The neutron transmission T_i in TOF channel i is given by

$$T_i = \frac{C_i^S - K_S B_i - B_S}{C_i^O - K_O B_i - B_O} \quad , \tag{3}$$

where

$C_i^S,\ C_i^O$ = dead-time–corrected and monitor-normalized counting rates for the sample and open measurements, respectively

B_i = unnormalized time-dependent background counting rate

B_S, B_O = steady-state background counting rates for the sample and open measurements, respectively

K_S, K_O = time-dependent background normalization factors for the sample and open measurements, respectively.

Note that the open sample for the liquid sample measurements is the equal-thickness D_2O sample, and the empty aluminum container is the open for the CsF sample measurements.

The determination of the time-dependent background is one of the more difficult tasks to accomplish. This background was determined by inserting into the beam a set of samples, called "notches," containing blacked-out resonances and then extrapolating to the sample and open conditions without the notch samples in the beam.[29] For the epithermal transmission measurements, a 0.635-cm-thick metallic Na sample was left in the beam to provide a permanent notch near 2.8 keV. Samples of Ag, W, and Co were cycled in the beam during the notch measurements with liquid samples to produce notches near 5.2, 18.6, and 132 eV, respectively. For the thermal measurements a 0.0178-cm-thick Ag sample was left permanently in the beam to produce a notch near 5.2 eV, and a package of Cd, In, and Ag samples was cycled into the beam to provide notches below 0.3 eV, near 1.45 eV, and near 5.2 eV, respectively.

For the CsF samples the transmission is that of the CsF and two sheets of Mylar. For the liquid samples the transmission is that of the Cs-containing liquid sample counting rate divided by the D_2O compensator sample counting rate.

IV. RESULTS

The transmission and capture data were analyzed for resonance parameters using the R-matrix Bayesian code SAMMY version 8 (Ref. 22). The analysis employed the experimental resolution, Doppler broadening, self-shielding, multiple scattering, and Reich-Moore approximation features of SAMMY. This code takes into account the statistical fluctuations in the experimental data points and known uncertainties in experimental parameters such as sample thickness, detector efficiency, flight path length, etc. Both the transmission and capture yield data were fitted, and a final set of resonance parameters was obtained for the best overall fit to all of the data. Only s-wave ($\ell = 0$) resonances were observed in this experiment, and thus, all results in this paper refer to s-wave resonances.

IV.A. Capture Yield and Transmission Plots

The capture and transmission thermal data are plotted in Figs. 1 and 2, and the epithermal data are plotted in Figs. 3 through 6. Figures 1 through 6 show the experimental capture yield and transmission data points, the SAMMY fit to all the data, and the corresponding ENDF/B-VIII.0 (Ref. 30) values. The SAMMY fit is shown as a solid line with the same color as the data points whereas the ENDF curves are shown as a dashed gray line.

The transmission data are not shown below 0.1 eV in Fig. 1 because the SAMMY code could not reproduce the large crystalline scattering effects in CsF below 0.1 eV. However, as can be seen in Fig. 1, the capture yield shows little crystalline effects and thus was analyzed by SAMMY down to 0.01 eV. In Fig. 2 there are no transmission data points near 5 eV. There is a silver fixed notch filter in the beam, which has a black resonance near 5 eV,

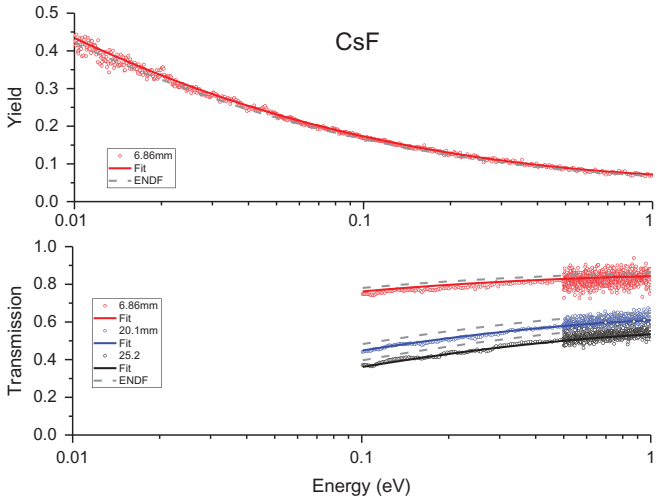

Fig. 1. Capture yield of CsF from 0.01 to 1 eV and transmission through CsF and Mylar from 0.1 to 1 eV for CsF samples. The transmission data below 0.1 eV are not shown as these data exhibited strong fluctuations due to crystalline scattering and could not be fitted by the SAMMY code. The 6.86-, 20.1-, and 25.2-mm labels refer to the CsF sample thicknesses, and the ENDF label refers to ENDF/B-VIII.0.

so data near 5 eV were excluded from the SAMMY analysis.

The epithermal results from 3 to 600 eV are plotted in Fig. 3. The resonances appear to be well separated from each other and thus should provide a good estimate of the average level spacing. Figure 4 shows the data near the 5.9-eV resonance. This is the lowest-energy s-wave resonance in Cs and is thus a major contributor to the Cs thermal capture cross section and resonance integral. Note that the new data show a resonance that lies at slightly lower energy than the ENDF resonance. Figures 5 and 6 illustrate the quality of the fits to the data where resonances are close together.

IV.B. Resonance Parameters

Table IV lists the resonance parameters obtained from the analysis of all the thermal and epithermal transmission and capture data. The SAMMY analysis accounted for the presence of fluorine in the CsF samples; the presence of Mylar in the CsF transmission samples; the presence of carbon, hydrogen, and oxygen in the Cs liquid samples; and the excess D_2O in the compensator samples used for the open beam transmission measurement of the liquid samples. For resonances below ~10 eV, where the resolution width is small or comparable to the total width, the radiation width can be obtained from the SAMMY fit to the resonances. Above ~10 eV, radiation widths were determined whenever a resonance included a significant quantity of scattering. The criterion of $\Gamma_\gamma/\Gamma_n < 5$ was adopted from Barry[27] to reflect the sensitivity for determining the radiation width from a SAMMY analysis of the resonance data. For resonances occurring above ~10 eV that produced an initial fit resulting in $\Gamma_\gamma/\Gamma_n > 5$, the radiation widths were set equal to their weighted average value for each spin state; the weighted average was determined from the radiation widths measured in this experiment. The resonance energies and radiation widths of the negative-energy resonances at −35.33 and

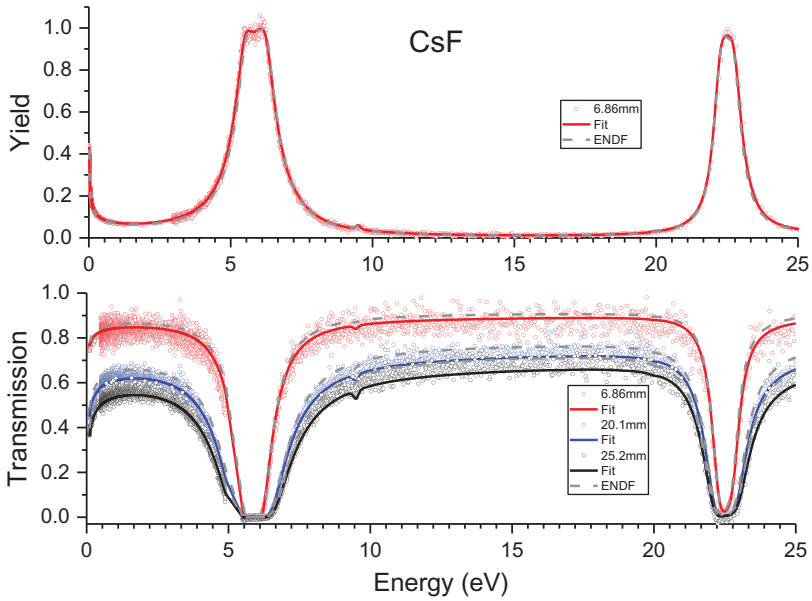

Fig. 2. Capture yield of CsF from 0.01 to 25 eV and transmission through CsF and Mylar from 0.1 to 25 eV. The 6.86-, 20.1- and 25.2-mm labels refer to the CsF sample thicknesses, and the ENDF label refers to ENDF/B-VIII.0.

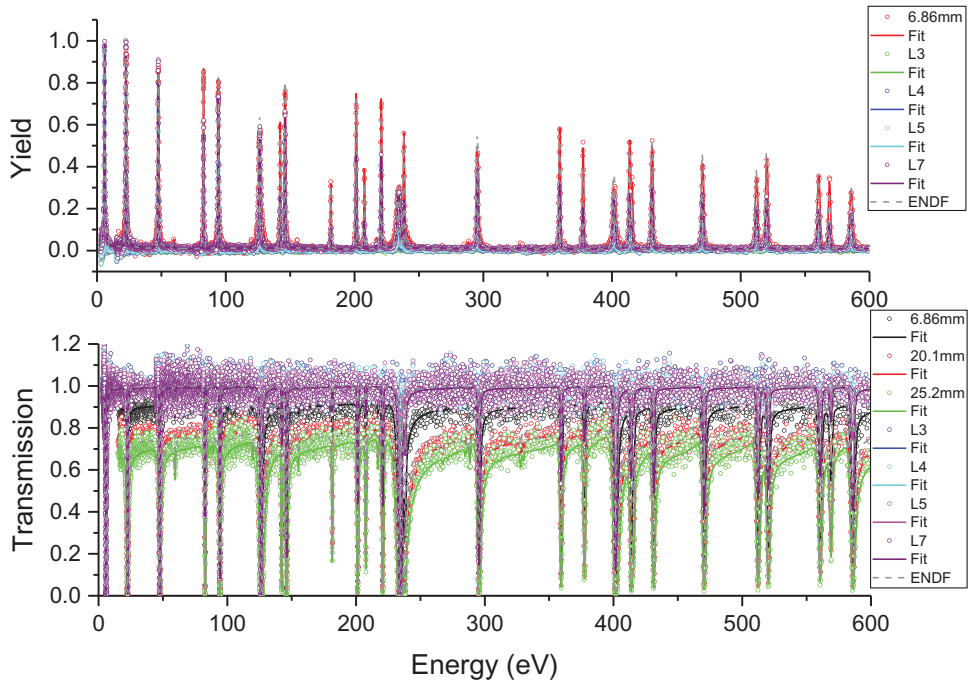

Fig. 3. Capture yield and transmission from 3 to 600 eV for Cs liquid and solid samples. The 6.86-, 20.1-, and 25.2-mm labels refer to the CsF sample thicknesses. The L3, L4, L5, and L7 labels refer to the liquid samples (see Table III). The ENDF label refers to ENDF/B-VIII.0.

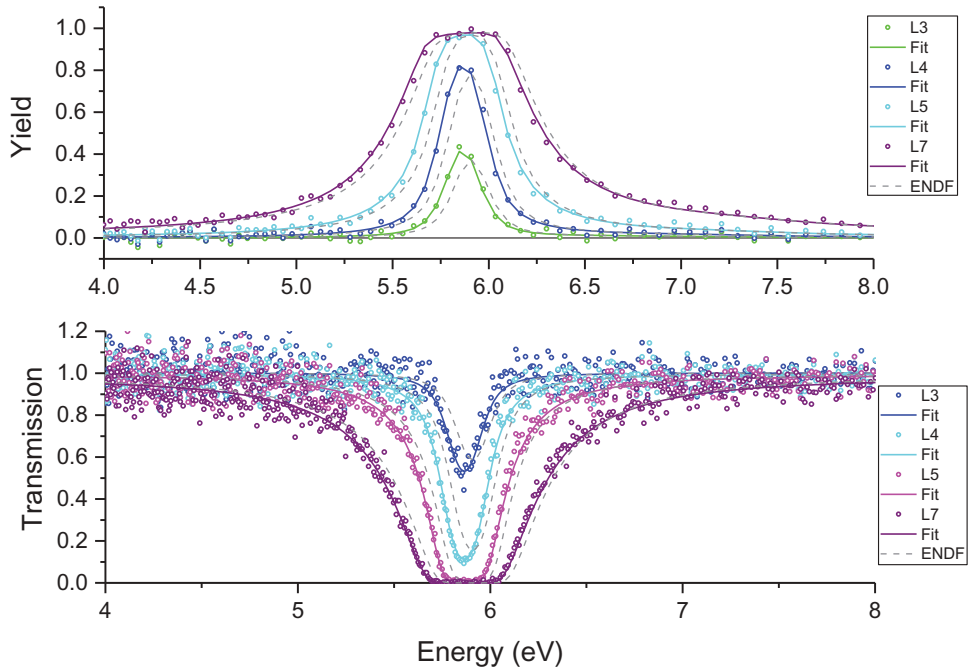

Fig. 4. Capture yield and transmission from 4 to 8 eV for Cs liquid samples. The L3, L4, L5, and L7 labels refer to the liquid samples (see Table III). The ENDF label refers to ENDF/B-VIII.0.

−13.63 eV were set equal to their ENDF (Ref. 30) values. The first two negative-energy resonances listed in Table IV were introduced to fit the transmission between resonances, a region dominated by potential scattering while keeping the effective radius R' equal to the ENDF value. This is based on the method introduced by Fröhner and Bouland.[31]

Table IV lists the SAMMY resonance energy E_o, radiation width Γ_γ, and neutron width Γ_n in columns 1, 5,

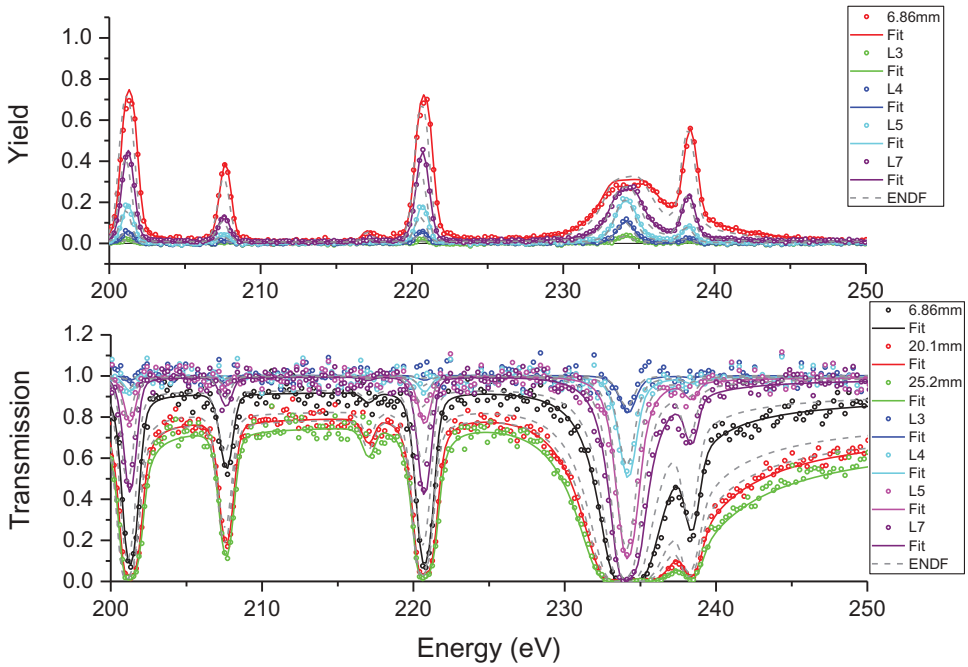

Fig. 5. Capture yield and transmission from 200 to 250 eV for Cs liquid and crystalline samples. The 6.86-, 20.1-, and 25.2-mm labels refer to the CsF sample thicknesses. The L3, L4, L5, and L7 labels refer to the liquid samples (see Table III). The ENDF label refers to ENDF/B-VIII.0.

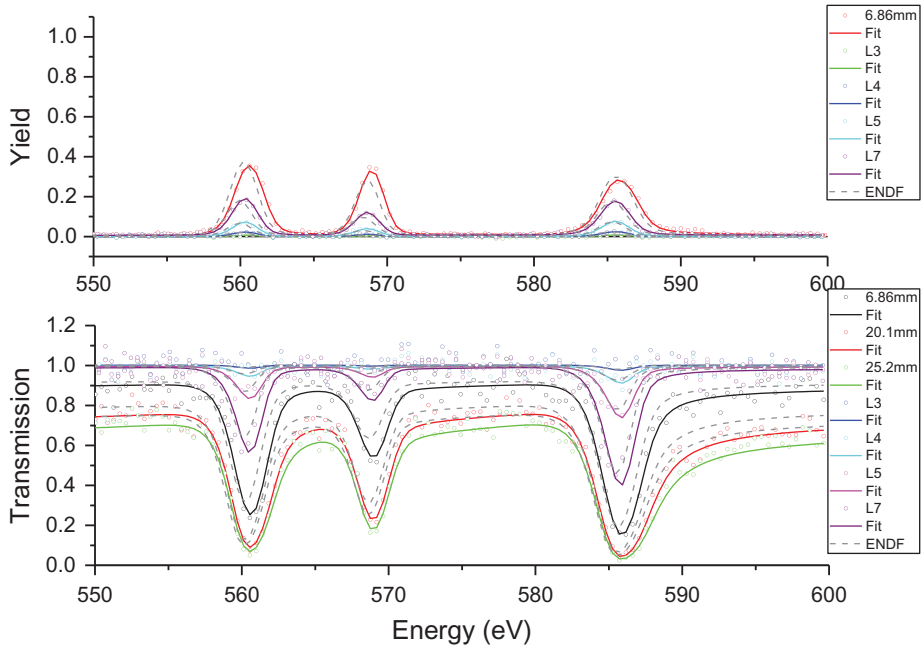

Fig. 6. Capture yield and transmission from 550 to 600 eV for Cs liquid and crystalline samples. The 6.86-, 20.1-, and 25.2-mm labels refer to the CsF sample thicknesses. The L3, L4, L5, and L7 labels refer to the liquid samples (see Table III). The ENDF label refers to ENDF/B-VIII.0.

and 9, respectively. The corresponding ENDF resonance parameters $E_{o,endf}$, $\Gamma_{\gamma,endf}$, and $\Gamma_{n,endf}$ are listed in columns 4, 8, and 12, respectively. The SAMMY (Bayesian) absolute uncertainties in the resonance parameters $\Delta E_{o,B}$, $\Delta\Gamma_{\gamma,B}$, and $\Delta\Gamma_{n,B}$ are listed in columns 2, 6, and 10, respectively. The external uncertainties $\Delta E_{o,ext}$, $\Delta\Gamma_{\gamma,ext}$,

TABLE IV

Cesium s-wave Resonance Parameters from the Combined Thermal and Epithermal Measurements*

E_o (eV)	$\Delta E_{o,B}$ (eV)	$\Delta E_{o,ext}$ (eV)	$E_{o,endf}$ (eV)	Γ_γ (meV)	$\Delta\Gamma_{\gamma,B}$ (meV)	$\Delta\Gamma_{\gamma,ext}$ (meV)	$\Gamma_{\gamma,endf}$ (meV)	Γ_n (meV)	$\Delta\Gamma_{n,B}$ (meV)	$\Delta\Gamma_{n,ext}$ (meV)	$\Gamma_{n,endf}$ (meV)	J
−192 368				120				3.64E+07				4
−50 572				120				9.06E+06				3
−35.33			−35.33	111			111	143	1.1	1	203.3	4
−13.63			−13.63	111			111	23	0.2	0.3	12.98	3
5.866	0.0003	0.001	5.91	117	0.5	5	120	7.2	0.03	0.2	6.41	3
22.516	0.0005	0.004	22.51	114			119	8.9	0.02	0.1	7.77	3
47.559	0.000	0.004	47.57	111	1	6	116	24	0.1	1	21.49	3
82.759	0.001	0.004	82.74	116			140	8.0	0.05	0.2	6.83	4
94.265	0.001	0.008	94.25	127	2	5	124	33	0.2	1	26.51	3
126.32	0.001	0.01	126.3	119	1	4	120	132	0.6	2	104.0	4
142.29	0.002	0.005	142.2	114			120	7.3	0.07	0.2	6.10	3
146.10	0.002	0.01	146	120	2	5	114	34	0.3	1	24.71	4
181.64	0.005	0.005	181.5	114			101	3.8	0.05	0.1	3.53	3
201.36	0.002	0.01	201.2	116	3	6	100	28	0.4	1	22.67	4
207.71	0.005	0.03	207.6	116			120	4.8	0.05	0.1	3.69	4
220.84	0.003	0.01	220.7	113	3	5	90	33	0.5	1	19.73	4
234.28	0.003	0.02	234.2	120	1	2	104	449	1	7	350.2	4
238.43	0.005	0.02	238.3	116			120	12	0.2	0.2	11.64	4
295.55	0.004	0.02	295.4	120	1	3	120	143	1	2	97.78	4
359.44	0.005	0.02	359.2	128	4	5	120	53	0.9	2	33.87	4
377.58	0.006	0.04	377.4	114			120	37	0.5	2	20.46	3
401.78	0.006	0.04	401.5	120	1	2	120	331	2	7	234.7	4
413.83	0.01	0.04	413.6	139	4	3	120	81	2	2	62.06	3
415.71	0.01	0.03	415.3	114			120	17	0.3	1	12.11	3
431.26	0.01	0.03	431	125	3	4	120	93	1	3	56.36	4
470.48	0.01	0.03	470.2	121	2	2	120	149	2	4	110.2	4
512.40	0.01	0.03	512.1	116	2	2	120	181	3	4	144.0	3
520.37	0.01	0.03	520.1	114	3	2	120	123	2	3	104.3	4
560.66	0.01	0.04	560.3	124	2	2	120	152	3	5	115.4	3
568.97	0.01	0.09	568.7	122	10	2	120	44	1	2	31.00	3
585.92	0.01	0.05	585.7	125	2	2	120	298	4	8	244.6	3

*Subscripts *B, ext*, and *endf* refer to final Bayesian uncertainties, external uncertainties, and ENDF/B-VIII.0 resonance parameters, respectively. Resonance spins J were taken from ENDF. The radiation widths that do not list Baysean and external errors were set to their weighted average for the positive energy resonances. The radiation widths of the −192 368- and −50 572-eV resonances were set equal to 120 meV, and the radiation widths of the −35.33- and −13.63-eV resonances were set to their ENDF values.

and $\Delta\Gamma_{n,ext}$ are listed in columns 3, 7, and 11, respectively. Column 13 lists the total angular momentum J of the resonances.

External uncertainties are a measure of the fluctuations in the resonance parameters when each of the 4 thermal measurements and each of the 12 epithermal measurements are individually solved by SAMMY with the same input parameters. For the combined thermal and epithermal analysis, the ENDF parameters were used as the starting point for each calculation.

The external uncertainty in E_o, Γ_γ, or Γ_n is determined from the mean-square deviation, Eq. (4):

$$\Delta X_{ext} = \sqrt{\left\{\sum_1^n \frac{(X_i - \langle X\rangle)^2}{(\Delta X_{B,i})^2}\right\} \Big/ \left\{(n-1)\sum_1^n \frac{1}{(\Delta X_{B,i})^2}\right\}}, \tag{4}$$

where

X = E_o, Γ_γ, or Γ_n

n = number of measurements (4 thermal and 12 epithermal)

$\Delta X_{B,i}$ = Bayesian SAMMY uncertainty in E_o, Γ_γ, or Γ_n for each sample i.

The weighted-average parameter $\langle X\rangle$ in Eq. (4) is determined from Eq. (5):

$$\langle X\rangle = \sum_1^n \frac{X_i}{(\Delta X_{B,i})^2} \Big/ \sum_1^n \frac{1}{(\Delta X_{B,i})^2} \, . \tag{5}$$

The deviations between samples, or external errors, are typically larger than those based on counting statistics, i.e., Bayesian errors. It is recommended that the larger of these two errors be used in applying these results.

IV.B.1. Parameter Distributions and Strength Function

The distributions of the widths of the fitted parameters were plotted. Sensitive radiation widths were plotted and fitted to a χ^2 distribution with 843 deg of freedom. This number of degrees of freedom was obtained through a least-squares error search. Neutron widths were converted into reduced neutron widths, which are defined in Ref. 32, and plotted alongside a distribution predicted by Porter-Thomas theory,[33] which claims neutron reduced widths are distributed via a χ^2 distribution with one degree of freedom. The radiation width distribution plot is given in Fig. 7, and the reduced neutron width distribution plot is given in Fig. 8. Also included in Fig. 8 is the distribution of reduced neutron widths from ENDF-B/VIII.0.

In addition to the distributions of widths, the strength function for the newly fitted parameters was computed and compared with the strength function computed from the parameters in ENDF/B-VIII.0 in the same energy range. The method used to calculate these values is the one given in Appendix A of Ref. 34, where plots of cumulative reduced neutron widths versus energy were made and the strength function was determined as the slope of the best-fit line of the plot. This plot is given in Fig. 9. Only the best-fit line for the parameters resultant from this measurement is shown in Fig. 9. In units of 10^{-4}, the strength function for ENDF parameters was 1.0 ± 0.3, and the strength function for the parameters from this measurement was 1.3 ± 0.4. This higher value of strength function is due to the increase in neutron widths obtained in this measurement relative to the ENDF widths.

IV.C. Thermal Capture Cross Section and Resonance Integral

The SAMMY-fit Bayesian resonance parameters listed in Table IV and ENDF parameters for resonances above 600 eV (including p-waves) were input to the NJOY nuclear data processing code[35] to obtain Doppler-broadened cross sections and the thermal capture cross section. From these cross sections, the capture resonance integral RI_γ was calculated from Eq. (6) utilizing the INTER utility code[36]:

$$RI_\gamma = \int_{0.5\text{eV}}^{20\text{MeV}} \sigma_\gamma(E)\frac{dE}{E} \, . \tag{6}$$

Uncertainties of thermal cross section and resonance integral were determined via a Monte Carlo method where the fitted resonance parameters were sampled from Gaussian distributions centered on the fitted resonance parameter values with standard deviations equal to the uncertainty of the fitted values. The thermal cross section and resonance integral were computed with each set of sampled resonance parameters. The mean values of the calculations were taken to be the thermal cross section and resonance integral, and the standard deviations of the calculation results were taken to be the uncertainties on these values.

These results, the corresponding ENDF values, and other published experimental values are listed in

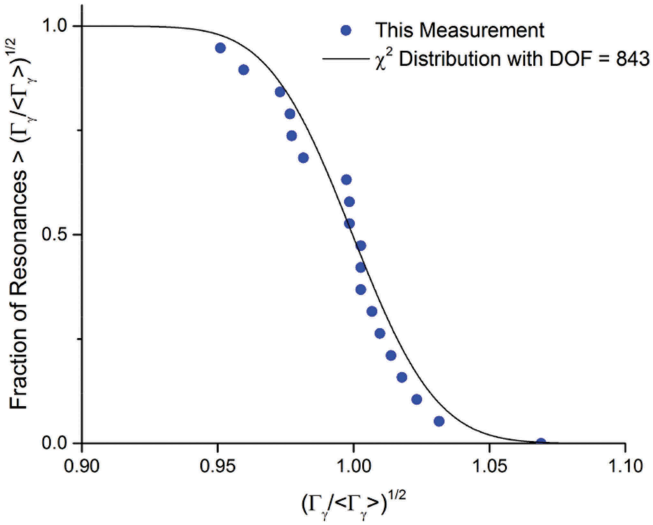

Fig. 7. Cumulative radiation width distribution for ^{133}Cs parameters from this measurement compared with a χ^2 distribution with 843 deg of freedom. The radiation widths in each spin state were normalized to the average radiation width for that spin state.

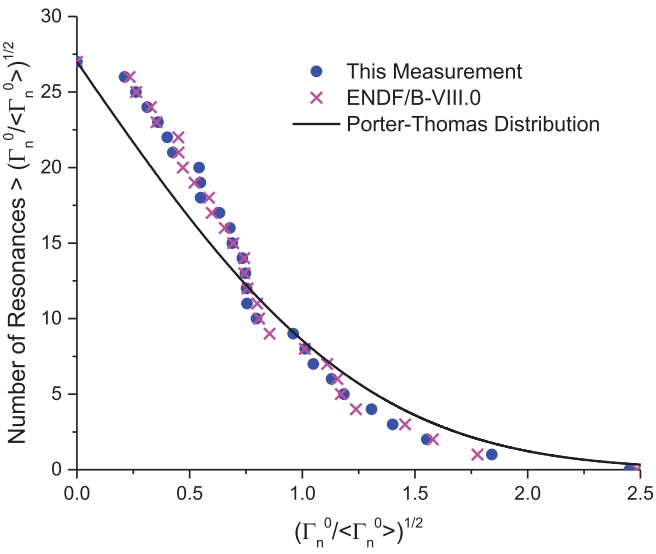

Fig. 8. Cumulative reduced neutron width distributions for ^{133}Cs parameters for this measurement and ENDF. These are plotted along with a Porter-Thomas distribution. The reduced neutron widths were normalized to the average for each spin state.

Table V for the ^{133}Cs thermal capture cross section and capture resonance integral. The 32.1 ± 0.9 b thermal capture cross section is higher than most of the other experimental values and lies about 3σ above the JENDL (Ref. 37) and ENDF and JEFF (Ref. 38) values. However, the thermal capture cross section

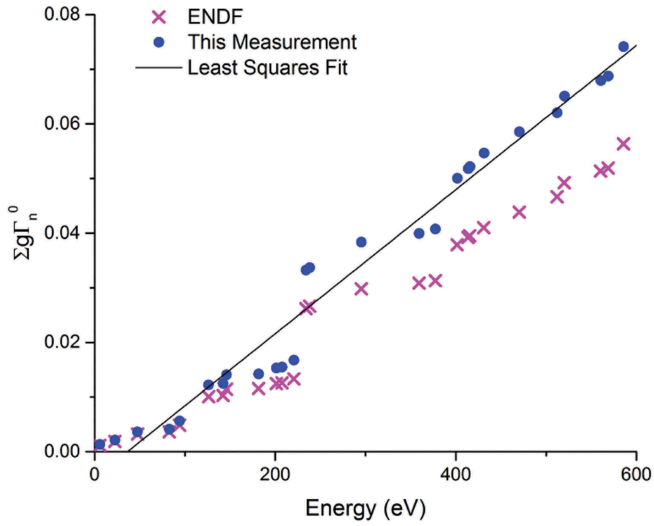

Fig. 9. Cumulative reduced neutron width versus energy for the parameters from ENDF and this measurement. In the plot the reduced neutron widths are scaled by the statistical weight factor *g*.

from this measurement is within 1σ of the recent Yoon and Lee[8] value of 31.2 ± 0.3 b. The 460 ± 10 b capture resonance integral agrees within uncertainties with the Baerg and Bartholomew[14] and Steinnes[19] values. The evaluations have no stated uncertainties, but the present measurement's capture resonance integral is slightly more than 1σ from JENDL and differs by almost 6σ from ENDF and 4σ from JEFF.

V. CONCLUSIONS

Capture and transmission measurements were carried out with liquid and solid samples of Cs from 0.01 to 600 eV. Resonance parameters were obtained for 4 negative-energy and 27 positive-energy resonances. The radiation width distribution from this measurement fits a χ^2 distribution with 843 deg of freedom. The cumulative reduced neutron width distribution compared favorably to a Porter-Thomas distribution.

The thermal capture cross section and capture resonance integral were determined from this measurement. The thermal capture cross section lies about 3σ above the ENDF, JENDL, and JEFF values. The capture resonance integral lies 1.4σ above the JENDL value, 5.5σ above the ENDF value, and 3.9σ above the JEFF value. An s-wave strength function of $(1.3 \pm 0.4) \times 10^{-4}$ was obtained for resonances below 600 eV.

TABLE V

Cesium-133 Neutron Thermal Capture Cross Section and Resonance Integral

Source	σ_γ (0.0253 eV) (b)	RI_γ (b)	Reference Number
This measurement	32.1 ± 0.9	460 ± 10	
Pomerance (1951)	29.0 + 1.5		10
Cummins (1957)	28.7 ± 0.7		11
Bayly et al. (1958)	30.4 ± 1.7		12
Bidinosti et al. (1958)	39.9 (effective cross section)	320	13
Baerg and Bartholomew (1960)	30.4 ± 0.8	461 ± 25	14
Tattersall et al. (1960)	28 ± 1		15
Brown et al. (1961)	33.4 ± 2.6 33.4 ± 3.2 32.9 ± 4.7	370 ± 50 375 ± 50 350 ± 80	16
Carre and Idal (1966)	28 ± 1		17
Sims and Junhke (1968)	29.2 ± 2.3	495 ± 17	18
Steinnes (1972)		437 ± 26	19
Takiue and Ishikawa (1978)	28.7 ± 0.7		20
Nakamura et al. (1999)	29.0 ± 1.0	298 ± 16	21
Yoon and Lee (2011)	31.2 ± 0.3		8
Shibata et al. (JENDL-4.0) (2011)	28.90	446.0	37
Brown et al. (ENDF/B-VIII.0) (2018)	29.04	405.1	30
Koning et al. (JEFF 3.2) (2011)	29.00	420.7	38

Acknowledgments

The authors gratefully acknowledge the Gaerttner LINAC Center staff for both operating the accelerator during these measurements and providing the mechanical and electronic assistance needed. The submitted manuscript has been authored by a contractor of the U.S. Government under contract No. DE-NR-0000031. Accordingly, the U.S. Government retains a non-exclusive, royalty-free license to publish or reproduce the published form of this contribution, or allow others to do so, for U.S. Government purposes.

References

1. *Nuclides and Isotopes: Chart of the Nuclides*, 17th ed., Knolls Atomic Power Laboratory (2010).
2. H. H. LANDON and V. L. SAILOR, "Slow Neutron Resonances in Cesium, Palladium and Gold," *Phys. Rev.*, **93**, 1030 (1954); https://doi.org/10.1103/PhysRev.93.1030.
3. J. A. HARVEY et al., "Spacings and Neutron Widths of Nuclear Energy Levels," *Phys. Rev.*, **99**, 10 (1955); https://doi.org/10.1103/PhysRev.99.10.
4. J. B. GARG, J. RAINWATER, and W. W. HAVENS, "Neutron Resonance Spectroscopy V, Nb, Ag, I and Cs," *Phys. Rev.*, **137**, 547 (1965); https://doi.org/10.1103/PhysRev.137.B547.
5. V. A. ANUFRIEV et al., "Resonance Parameters of ^{133}Cs. ^{134}Cs($T_{1/2}$ = 2.2yr) in the Energy Range up to 400 eV." *Proc. Int. Conf. Interaction of Neutrons with Nuclei*, Lowell, Massachusetts, July 1976.
6. JU. P. POPOV and F. L. SHAPIRO, "Energy Dependence of Cross Sections for (*n, gamma*)

Reactions on a Number of Odd-Z Nuclei," *J. Soviet Phys. JETP*, **15**, 683 (1962).

7. F. WIDDER, Report No. 217, Eidgenössisches Institut für Reaktorforschung Würenlingen (1975).
8. J. YOON and S. LEE, "A Study on the Energy-Dependent Neutron-Capture Cross-Section of Natural Cesium (^{133}Cs) by Using a Continuous Neutron Flux," *New Phys.: Sae Mulli (Korean Phys. Soc.)*., **61**, 7 (2011).
9. G. D. HICKMAN, *Bull. Amer. Phys. Soc.*, **10**, 12 (1965).
10. H. POMERANCE, "Thermal Neutron Capture Cross Sections," *Phys. Rev.*, **83**, 641 (1951); https://doi.org/10.1103/PhysRev.83.641.
11. J. D. CUMMINS, Report No. 2333, Atomic Energy Research Establishment Harwell (1957).
12. J. G. BAYLY et al., "The Cross-Section of the Reaction ^{134}Cs(n,γ)^{135}Cs and the Half-Life of ^{134}Cs," *J. Inorg. Nucl. Chem.*, **5**, 259 (1958); https://doi.org/10.1016/0022-1902(58)80002-0.
13. D. R. BIDINOSTI, H. R. FICKEL, and R. H. TOMLINSON, *Proc. 2nd Int. Conf. Peaceful Uses of Atomic Power*, Geneva, Switzerland, September 1–13, 1958, Vol. 15, p. 459 (1958).
14. A. P. BAERG and R. M. BARTHOLOMEW, "Note on the Thermal Neutron Capture Cross Section of ^{133}Cs," *Can. J. Chem.*, **38**, 2528 (1960); https://doi.org/10.1139/v60-345.
15. R. B. TATTERSALL et al., "Pile Oscillator Measurements of Resonance Absorption Integrals," *J. Nucl. Energy A*, **12**, 32 (1960); https://doi.org/10.1016/0368-3265(60)90006-2.
16. F. BROWN, P. J. CAMPION, and B. H. OLIVER, "The Cross-Section for the Reaction ^{133}Cs(n,γ)^{134}Cs in the NRX Reactor," *J. Nucl. Energy A*, **13**, 141 (1961); https://doi.org/10.1016/0368-3265(61)90005-6.
17. J. V. CARRE and R. IDAL, "Measurement of Cross Sections and Resonance Integrals by the Pile Oscillator Method," *Proc. Conf. Nuclear Data for Reactors*, Paris, France, October 17–21, 1966, Vol. 1, p. 479 (1966).
18. G. H. E. SIMS and D. G. JUNHKE, "The Thermal Neutron Cross-Sections and Resonance Integrals of ^{50}Cr, ^{109}Ag, ^{123}Sb, ^{133}Cs, ^{191}Ir and ^{201}Hg," *J. Inorg. Nucl. Chem.*, **30**, 349 (1968); https://doi.org/10.1016/0022-1902(68)80459-2.
19. E. STEINNES, "Resonance Activation Integrals of Some Nuclides of Interest in Neutron Activation Analysis," *J. Inorg. Nucl. Chem.*, **34**, 2699 (1972); https://doi.org/10.1016/0022-1902(72)80572-4.
20. M. TAKIUE and H. ISHIKAWA, "Thermal Neutron Reaction Cross Section Measurements for Fourteen Nuclides with a Liquid Scintillator Spectrometer," *Nucl. Instrum. Meth.*, **148**, 157 (1978); https://doi.org/10.1016/0029-554X(78)90347-6.
21. S. NAKAMURA, H. HARADA, and T. KATOH, "Measurement of Thermal Neutron Capture Cross Section and Resonance Integral of the Reaction ^{133}Cs(n,γ), ^{134m,134g}Cs," *J. Nucl. Sci. Technol.*, **36**, 847 (1999); https://doi.org/10.1080/18811248.1999.9726275.
22. N. M. LARSON, "Updated User's Guide for SAMMY: Multilevel R-Matrix Fits to Neutron Data Using Bayes Equations," ORNL/TM-9179/R8 ENDF-364/R2, Oak Ridge National Laboratory (Oct. 2008).
23. G. LEINWEBER et al., "Europium Resonance Parameters from Neutron Capture and Transmission Measurements in the Energy Range 0.01-200 eV," *Ann. Nucl. Eng.*, **69**, 74 (2014); https://doi.org/10.1016/j.anucene.2014.01.041.
24. Y. DANON, R. E. SLOVACEK, and R. C. BLOCK, "The Enhanced Thermal Neutron Target at the RPI LINAC," *Trans. Am. Nucl. Soc.*, **68**, 473 (1993).
25. Y. DANON, R. E. SLOVACEK, and R. C. BLOCK, "Design and Construction of a Thermal Neutron Target for the RPI LINAC," *Nucl. Instrum. Meth. Phys. Res. A*, **352**, 596 (1995); https://doi.org/10.1016/0168-9002(95)90012-8.
26. M. E. OVERBERG et al., "Photoneutron Target Development for the RPI Linear Accelerator," *Nucl. Instrum. Meth. Phys Res. A*, **438**, 253 (1999); https://doi.org/10.1016/S0168-9002(99)00878-5.
27. D. P. BARRY, "Neodymium Neutron Transmission and Capture Measurements and Development of a New Transmission Detector," PhD Thesis, Rensselaer Polytechnic Institute (2003).
28. R. C. BLOCK et al., "A Multiplicity Detector for Accurate Low-Energy Neutron Capture Measurements," *Proc. Int. Conf. Nuclear Data for Science and Technology*, Mito, Japan, May 30–June 3, 1988, p. 383; https://doi.org/10.3168/jds.S0022-0302(88)79586-7.
29. D. B. SYME, "The Black and White Filter Method for Background Determination in Neutron Time-of-Flight Spectrometry," *Nucl. Instrum. Meth. Phys. Res.*, **198**, 357 (1982); https://doi.org/10.1016/0167-5087(82)90276-9.
30. D. A. BROWN et al., "ENDF/B-VIII.0: The 8th Major Release of the Nuclear Reaction Data Library with CIELO-Project Cross Sections, New Standards and Thermal Scattering Data," *Nucl. Data Sheets*, **148**, 1 (2018); https://doi.org/10.1016/j.nds.2018.02.001.
31. F. FRÖHNER and O. BOULAND, "Treatment of External Levels in Neutron Resonance Fitting: Application to the Nonfissile Nuclide ^{52}Cr," *Nucl. Sci. Eng.*, **137**, 70 (2001); https://doi.org/10.13182/NSE01-A2176.
32. S. F. MUGHABGHAB, *Atlas of Neutron Resonances: Resonance Parameters and Thermal Cross Sections Z = 1-100*, Elsevier, Amsterdam, Netherlands (2006).
33. C. E. PORTER and R. G. THOMAS, "Fluctuations of Nuclear Reaction Widths," *Phys. Rev.*, **104**, 483 (1956); https://doi.org/10.1103/PhysRev.104.483.

34. G. LEINWEBER et al., "Cadmium Resonance Parameters from Neutron Capture and Transmission Measurements of Cadmium at the RPI LINAC," arXiv:1801.03424vl [nucl-ex], Cornell University (2018).

35. R. MacFARLANE and D. MUIR, "The NJOY Nuclear Data Processing System," Version 91, LA-12740-M, Los Alamos National Laboratory (1994).

36. C. L. DUNFORD, "ENDF Utility Codes Release 6.12," Informal Report, Brookhaven National Laboratory (2001).

37. K. SHIBATA et al., "JENDL-4.0: A New Library for Nuclear Science and Engineering," *J. Nucl. Sci. Technol.*, **48** (2011); https://doi.org/10.1080/18811248.2011.9711675.

38. A. J. KONING et al., "Status of the JEFF Nuclear Data Library," *J. Korean Phys. Soc.*, **59**, *2*, 1057 (2011).